New Zealand Journal of Geology and Geophysics

ISSN: (Print) (Online) Journal homepage: www.tandfonline.com/journals/tnzg20

Tridymite formation as a direct consequence of explosive volcanism – evidence preserved in tuffisite veins and concurrently erupted volcanic ash

Andreas Auer, Alexander Belousov, Marina Belousova, Hiroshi Kitagawa & Katsura Kobayashi

To cite this article: Andreas Auer, Alexander Belousov, Marina Belousova, Hiroshi Kitagawa & Katsura Kobayashi (01 Dec 2024): Tridymite formation as a direct consequence of explosive volcanism – evidence preserved in tuffisite veins and concurrently erupted volcanic ash, New Zealand Journal of Geology and Geophysics, DOI: 10.1080/00288306.2024.2430556

To link to this article: https://doi.org/10.1080/00288306.2024.2430556

Published online: 01 Dec 2024.

NEW ZEALAND JOURNAL OF GEOLOGY AND GEOPHYSICS
https://doi.org/10.1080/00288306.2024.2430556

Taylor & Francis
Taylor & Francis Group

RESEARCH ARTICLE

Tridymite formation as a direct consequence of explosive volcanism – evidence preserved in tuffisite veins and concurrently erupted volcanic ash

Andreas Auer [a], Alexander Belousov[b], Marina Belousova[b], Hiroshi Kitagawa[c] and Katsura Kobayashi[c]

[a]Department of Geoscience, Shimane University, Matsue, Japan; [b]Institute of Volcanology and Seismology, Petropavlovsk-Kamchatsky, Russia; [c]Pheasant Memorial Laboratory, Institute for Planetary Materials, Okayama University, Misasa, Tottori, Japan

ABSTRACT

The mineralogy of volcanic rocks is usually considered as a consecutive crystallisation path related to a liquid line of decent. Tephra and pyroclastic rocks hold a special status as their formation includes the physical disruption of the magma during an explosive eruption. We describe tuffisite samples (captured veins of pyroclastic material in coherent lava bombs) and concurrently ejected volcanic ash from the ongoing eruption of Ebeko Volcano, Russia. Our samples show that tridymite (a mineral, not present in the original phase assemblage of the magma) forms as a consequence of explosive eruptive activity, volatile exsolution and fluid flow following decompression and magma fragmentation. Vapour phase crystallisation (VPC) of cristobalite is well known from highly evolved, dome-forming eruptions due to gas flux through highly permeable and porous glassy dome rocks. At Ebeko volcano, increased permeability develops in the volcanic conduit during magma fragmentation and transient tephra storage. Magmas erupted at Ebeko are less evolved than those of typical (dome-forming) andesitic – dacitic Peléan eruptions and show comparably higher eruption temperatures favouring the formation of tridymite over cristobalite during VPC.

ARTICLE HISTORY
Received 17 July 2024
Accepted 7 November 2024

HANDLING EDITOR
Yoshihiko Tamura

KEYWORDS
Tridymite; tuffisite; vulcanian explosive eruption; magmatic fragmentation; silicosis; volcanic ash; tephra; silica polymorph; Ebeko volcano

Introduction

A Vulcanian explosion initiates when a conduit seal ruptures, and a decompression wave travels into pressurised upper crustal magma. This leads to physical disruption of the magma into fragments of various sizes (Clarke et al. 2015). During this process a continuous liquid phase (magma = melt ± gas bubble, ± crystals) is transformed into a gas phase with dispersed fragments known as 'pyroclasts' (Cashman and Scheu 2015). Although fragmentation mechanisms have been reproduced in laboratory experiments (Alidibirov and Dingwell 1996; Martel et al. 2000; Martel et al. 2001; Spieler et al. 2004), and inferred from indirect observation (Muramatsu et al. 2023), a direct observation of these processes in nature is precluded by the inherent danger of explosive eruptions. A spectacular exception to this rule is subject of this work. We describe tuffisite samples from the 2019 eruption of Ebeko volcano in the Kurile Island Arc, which have recorded cycles of fragmentation, fluid flow and sintering during ongoing Vulcanian style activity. Tuffisites are pyroclastic rocks which occur as veins, bands or discordantly cross cutting fractured networks either injected into adjacent host rock (external tuffisite) or within the active magma body (internal tuffisite) (Unwin et al. 2021). The term has no genetic implication and has been described in relation to diatremes (Cloos 1942), from active (Noguchi et al. 2008) and exhumed conduits (Tuffen et al. 2003) and from erupted products of silica rich (rhyolitic) eruptions (Kendrick et al. 2016; Schipper et al. 2021; Unwin et al. 2023).

During an active Vulcanian explosion magma gets fragmented and pyroclasts are transported into a gas phase and ejected into the atmosphere, forming a volcanic plume. If, however some of the fragmented material is entrained or injected into the coherent surrounding magma and preserved, it will form an internal tuffisite and thus provide frozen evidence of an episode of the explosive magma disruption (Kendrick et al. 2016; Unwin et al. 2021). Our samples show that fluid percolation through pyroclastic material, following magmatic fragmentation enables tridymite crystallisation in the most finely fragmented pyroclastic material, a phase not originally present in the magma. Silica and other silica polymorphs (including cristobalite and tridymite) in volcanic ash are potentially hazardous to human health, especially with respect for the development of long-term respiratory problems such as silicosis (Horwell et al. 2008; Baxter et al. 2014). While the formation of the silica polymorph cristobalite in volcanic rocks has previously been linked mainly to vapour phase precipitation during lava flow and (crypto) dome growth (Hoblitt and Harmon 1993; Baxter et al. 1999; Boudon et al. 2015; Schipper et al. 2020). The occurrence of tridymite as another polymorph has been reported from

CONTACT Andreas Auer auer@riko.shimane-u.ac.jp

dome-forming eruptions at Soufriere Hills Volcano (Baxter et al. 1999), within erupted products from Hakone Volcano (Kuno 1950), Montagne Pele´e (Westercamp 1975) and Bezymianny Volcano (Davydova et al. 2022), as well as vapour-phase alteration after the eruption (Heled et al. 2022). Our study is

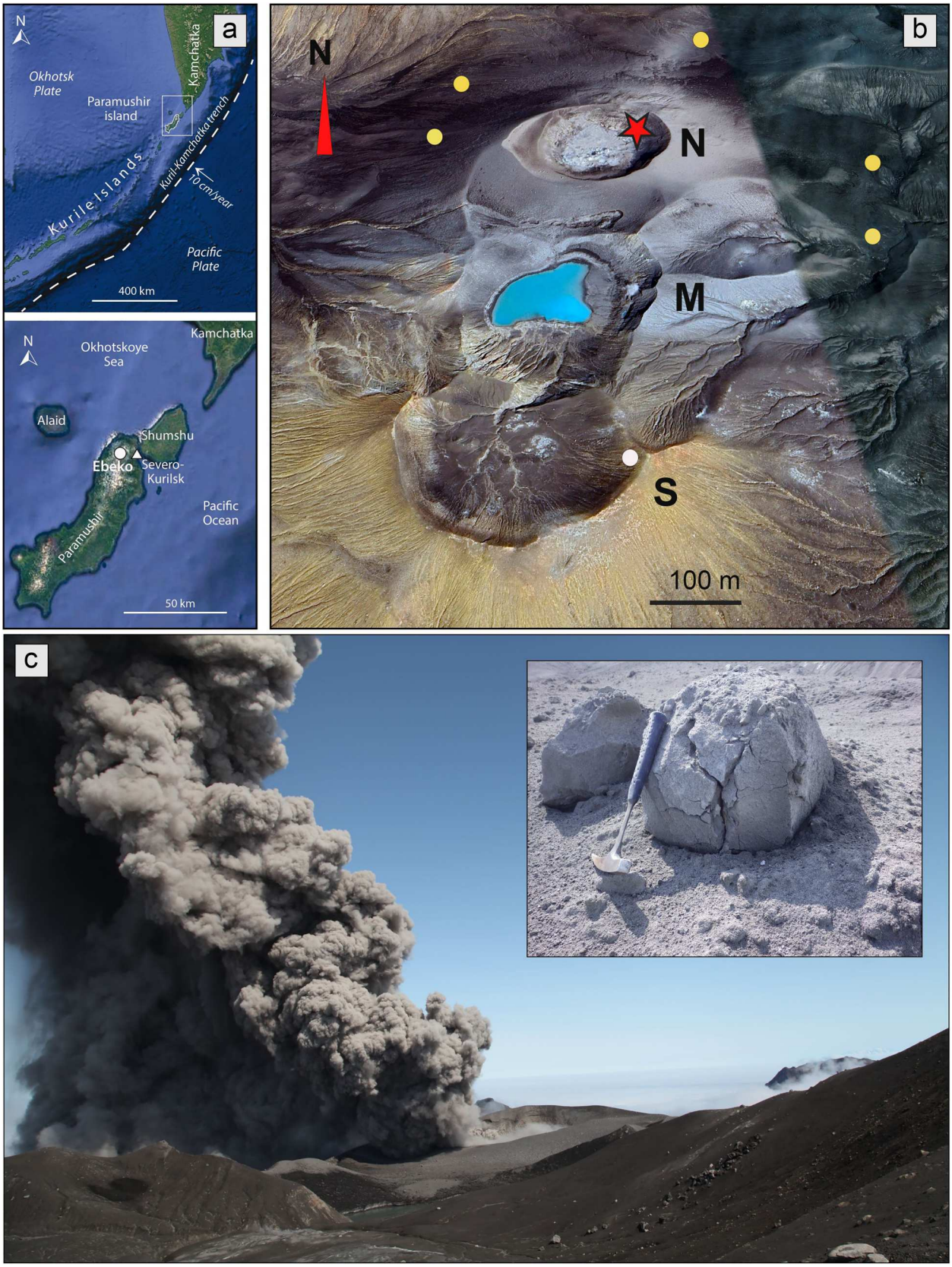

Figure 1. A, Tectonic setting and geographic location of Ebeko volcano **B,** Google Earth image showing the morphology of the summit area of Ebeko volcano with 3 craters: N – Northern, M – Middle, S – Southern crater. The star indicates place the current vent location from where the explosions occurred in 2019, yellow dots show sampling sites of bread-crust bombs and white dot shows the sampling site of ash collected directly from the eruption cloud **C,** Vulcanian explosion with a more than 500 m high eruption column at 14:42 on July14, 2019. The inset shows a fresh 'breadcrust' bomb.

the first account where tridymite formation can be directly linked to magmatic fragmentation during explosive volcanic eruptions. We use qualitative and quantitative textural analysis to characterise the fragmentation process and backscatter electron imaging and electron microprobe and micro-Raman analysis to document tridymite formation in tuffisite veins and concurrently erupted volcanic ash.

Ebeko Volcano and its ongoing eruption

Ebeko Volcano (1145 m above sea level) is located in the northern part of Paramushir Island and is one of the most active volcanoes of the Kurile Islands (Figure 1A). The edifice of Ebeko has no prominent, well-developed volcanic cone and the summit area is relatively flat and characterised by a row of three maar-like craters with diameters between 200–300 m (Figure 1B). Modern eruptive activity of Ebeko is characterised by prolonged (up to several years long) explosive eruptions that consist of separate ash-laden outbursts, mechanisms of which range from purely magmatic to phreatic/hydrothermal (Walter et al. 2020).

The volcano summit and its upper slopes are hydrothermally active with multiple fumaroles and boiling mud pools. 7 km to the east of the volcano the small town Severo-Kurilsk is located with a population of 2700 inhabitants. During active eruptive phases frequent ashfalls as well as elevated concentrations of volcanic gases in the air pose a threat to the town's population.

The latest eruption of the volcano started in 2016 and continues until the time of writing. This eruption consists of sporadic short-lived Vulcanian outbursts from the new northern crater (Belousov et al. 2021). Up to 120 explosions per month were registered during the summer months of 2020 and 2021 (Degterev and Chibisova 2022). The interval between the explosions varies from several minutes up to several days. The resulting ash-laden eruptive clouds rise to heights of about 1–2 km, in some cases up to 5 km above sea level. Together with ash, more coarse-grained materials were also balistically ejected as volcanic bombs of bread-crust type up to 1 m across which represent juvenile material of the eruption (Figure 1C).

Methods

Sampling and petrography

Fresh pyroclasts were sampled between July 9th and 15th 2019. Volcanic bombs were taken from freshly formed bomb sags on the outer slopes of the active new north crater (Walter et al. 2020). The bombs were ejected directly before sampling (still warm and not covered by fresh ash of the recent ashfalls) and fresh ash was collected following discrete explosions at a distance of 600 m from the vent (Belousov et al. 2021). Ten large Vulcanian bombs (of which 3 tuffisite veins were found) were cut for textural observation and preparation of 25 petrographic thin sections. Image nests at different magnifications were taken from adjacent areas in coherent magmatic domains and fragmental tuffisite, using a flatbed scanner and a petrographic microscope.

Images were taken under circular polarised light using commercially available quarter waveplates for the optical microscope to maximise plagioclase interference colours (Higgins 2010). After (semiautomatic) image enhancement, using Corel Draw and ImageJ, binary images of plagioclase and vesicles were obtained from adjacent lava and tuffisite domains (see supplementary file S2-4). Vesicularity per area was determined area using threshold functions of Corel Draw and ImageJ but also required manual corrections and enhancement afterwards. This requires that versicles have relative equant dimensions an assumption that is appropriate for our samples. Crystal size distribution (CSD) analysis (Higgins 2006) was limited to plagioclase because this phase is by far the most abundant, and digitalisation and image colour thresholding for this phase can be made most reliably (with respect to other crystal phases). Binary images were further processed by the software CSD corrections (Higgins 2000) to obtain crystal size distribution data. Vesicularity data (also obtained by image analysis) was considered in each calculation.

Ash samples were sieved and size fractions for coarse ash 710–1000 µm, fine ash 125–250 µm and very fine ash 63–125 µm were mounted in Epoxy resin and subsequently prepared as polished thin sections and grain mounts.

Major and trace element geochemistry, electron microprobe and micro Raman analysis

Major-element compositions of the Ebeko samples (n = 5) were analysed by an X-ray fluorescence spectrometry with a PAnalytical (present Malvern Panalytical) Axios Advanced instrument. Samples were fused with lithium tetraborate (Li2B4O7) flux (1: 10 = Wsample and Wflux) to form glass beads after Nguyen et al. (2020). Calibration was performed using GSJ standard rocks [JA-2, JA-3, JB-1b, JB-2, JB-3, JG-1a, JG-2, JGb-1, JGb-2, JH-1, JP-1, JR-1, JR-2 and JR-3] where A, B, G, Gb, H, P and R denote andesite, basalt, granite, gabbro, hornblendite, peridotite and rhyolite, respectively; Imai et al. (1995; 1999) and Terashima et al. (1998). Correction of matrix effects follows the fundamental parameter algorithm. The loss on ignition (LOI, weight loss by structural water release, and weight gain by iron oxidation) and H2O – (loss of adsorbed water) were determined gravimetrically (Nguyen et al. 2020). Temperatures applied to samples

for LOI and H2O – determinations are 1000 and 110 °C, respectively. All analyses were duplicated, and the relative difference among duplicates for a sample is better than 1%.

Trace-element compositions of the samples were analysed by an inductively coupled plasma-mass spectrometry with a Thermo Scientific iCAP TQ. Samples for determination of Li, Be, Rb, Sr, Y, Cs, Ba, La, Ce, Pr, Nd, Sm, Eu, Gd, Tb, Dy, Ho, Er, Tm, Yb, Lu, Pb, Th and U were decomposed with HF-HClO4 following Yokoyama et al. (1999). Samples for determination of Zr, Nb, Hf and Ta were decomposed with HF following Lu et al. (2007). The isotope-dilution internal standardisation methods were employed for determination of element abundances (Makishima and Nakamura 2006; Lu et al. 2007). All analyses were duplicated, and the relative difference among duplicates for a sample is better than 5%.

Backscatter electron images of tuffisite and ash samples were taken using an electron microprobe (JEOL 8530F) at Shimane University using 15 kV acceleration voltage and beam currents between 10 and 20 nA. Tridymite compositions were analysed by wavelength dispersive spectroscopy using the same instrument with 15 kV and 20 nA and a defocussed beam. The standards of synthetic and natural minerals and glasses from the Smithsonian Institute were used for calibration and monitoring of analytical quality. Element maps were prepared using a focussed beam of 15 kV and 20 nA and a step size between ¼ and 1 µm and a dwell time of 80 ms. Intensities were recalculated as element concentrations using measured standard concentrations and a ZAF matrix correction. In addition tridymite crystals were qualitatively analysed using energy dispersive spectroscopy to confirm if a respective phase in question is a silica polymorph.

More than 60 Raman spectra were collected for the tuffisite and ash samples to identify the silica polymorph using a Thermo Fisher Scientific DXR Raman microscope at Pheasant Memorial Laboratory, Institute for Planetary Materials, Okayama University, equipped with a Nd-YVO4 laser source and a wavelength of 532 nm. The laser power was 5 mW with a spatial resolution of ca 0.7 µm, diffraction grating of 900 line-per-mm and a spectrographic aperture 25 µm pinhole.

Results

Tuffisite and ash samples – composition, textures and crystal size distribution

Ebeko Volcano erupts highly porphyritic (47–56 vol% crystals) two-pyroxene basaltic andesites and andesites (Belousov et al. 2021). We analysed two samples from a magmatic domain, two samples from a tuffisite domain and one sample of fresh ash directly collected from a discrete explosive event. Standard deviation for major and trace elements among all textural types is very low suggesting a common magmatic source for all samples (Table 1). Phenocryst minerals consist of plagioclase, clinopyroxene, orthopyroxene, Fe-Ti oxide minerals, and rare olivine. Detailed modal proportions are also shown in Table 1. The hyalopilitic groundmass is either colourless or has a light brownish colour with abundant microlites of plagioclase and pyroxene (see supplement S1 for a representative, tuffisite free sample). Groundmass glass composition is rhyolitic (Table 2) with average silica content of about 75 wt% (Belousov et al. 2021). On the other hand, tuffisite veins have an ash grey colour and a dull, lustreless surface appearance. Using optical microscopy, there is a strong visual contrast between the coherent domains and the tuffisite domains (Figure 2, S2-1). The latter vary in thickness between a few mm and a few cm, often showing undulatory wavy contacts with the surrounding lava and contain intricate fluidal structures or even small folds. The main mineral constituents and proportions between the coherent magmatic domains and the tuffisite and ash samples are similar (Table 1) with the exception of tridymite in the tuffisite and ash. Glass in the magmatic domains is translucent whereas the tuffisite groundmass is indistinct and not clearly resolved by optical microscopy. At high-resolution backscatter images, the fragmental nature of the tuffisite and ash samples is also visible. Some of the tuffisite and ash samples show localised corrosion features (see S3-3). Plagioclase in magmatic domains is generally euhedral and shows prismatic and sometimes acicular habits (Figure 2). On the other hand, plagioclase in tuffisite veins is smaller, often highly fragmental, comprised of disjointed (but formerly euhedral) crystal pieces (Figure 2, S2-2. S2-3).

Vesicle textures in coherent magmatic clasts are usually smooth showing spherical or subspherical outlines. Isolated vesicles are usually equant or only slightly elongated but often two or several vesicles have coalesced. In contrast, vesicularity in the tuffisite is generally lower and vesicle textures show squashed and ragged outlines (S2-3). Within the tuffisite domains, individual larger glassy fragments are occasionally preserved and hosted within the fine-grained tuffisite matrix (Figure 3A, B). The tuffisites have corresponding counterparts in the erupted ash particles. Approximately 75% of the ash particles are pristine glassy fragments (Figure 3C upper image). The remaining 25% are either composite fragments (3c middle image) or finegrained fragmental clasts which are textural identical to the tuffisites (Figure 2, Figure 3C lower image, Figure 5 and S3).

Plagioclase CSD in coherent magmatic samples shows a slightly convex function generally typical for

Table 1. Modal composition and whole rock and trace element composition for Ebeko samples.

Modal glass (matrix for tuffisite) and mineral proportions for magmatic domains (MD), tuffisite and ash								
	MD1	MD2	MD3	MD4	MD5	Tuffisite 1	Tuffisite 2	Ash
Glass / Matrix	44	44	46	53	45	64	47	43
Plagioclase	38	39	39	29	39	21	34	39
Clinopyroxene	8	7	7	11	8	8	9	8
Orthopyroxene	8	7	6	5	5	3	4	6
Oxide	3	2	2	3	3	4	5	4
Olivine	tr	tr	tr	tr	tr	–	–	–
SUM	100	100	100	100	100	100	100	100

Major (and trace) element compositions of volcanic rocks from Ebeko volcano.						
	Coherent Lava Domain		Ash	Tuffisite		
Sample	EB-1	EB-2	EB-ASH	EB-TF-1	EB-TF-2	*St.Dev*
Major element oxides (wt%)						
SiO_2	58.60	59.20	57.52	58.51	58.33	*0.54*
TiO_2	0.65	0.64	0.69	0.68	0.67	*0.02*
Al_2O_3	17.00	16.52	16.59	16.77	16.90	*0.18*
Fe_2O_3*	7.89	7.87	8.38	8.13	8.03	*0.19*
MnO	0.18	0.17	0.17	0.18	0.17	*0.00*
MgO	3.07	2.97	3.23	3.14	3.13	*0.08*
CaO	7.37	6.86	7.12	7.20	7.31	*0.18*
Na_2O	3.09	3.03	2.80	2.95	2.97	*0.10*
K_2O	2.16	2.28	2.02	2.11	2.07	*0.09*
P_2O_5	0.19	0.17	0.18	0.18	0.18	*0.01*
LOI	0.01	0.07	0.65	−0.12	−0.07	*0.28*
H_2O^-	0.13	0.19	0.08	0	0	*0.08*
Total	100.35	99.99	99.44	99.71	99.68	
Trace element (ppm)						
Li	11.2	12.3	10.4	10.6	10.8	*0.65*
Be	0.747	0.778	0.646	0.639	0.689	*0.05*
Rb	48.1	53.6	45.9	47.8	47.1	*2.65*
Sr	449	428	436	451	454	*10.06*
Y	21.3	21.4	20.7	20.7	20.6	*0.33*
Zr	96.8	102	88.0	90.4	90.7	*4.99*
Nb	2.05	2.07	2.03	2.01	1.96	*0.04*
Cs	2.54	2.95	2.41	2.42	2.47	*0.20*
Ba	408	434	385	405	405	*15.41*
La	11.4	11.7	10.9	11.3	11.3	*0.28*
Ce	26.6	27.4	25.5	26.3	26.6	*0.60*
Pr	3.61	3.65	3.45	3.56	3.58	*0.07*
Nd	16.5	16.6	15.8	16.3	16.3	*0.27*
Sm	3.94	3.88	3.78	3.84	3.89	*0.05*
Eu	1.06	1.04	1.02	1.05	1.07	*0.02*
Gd	4.10	4.03	3.96	3.99	3.96	*0.05*
Tb	0.644	0.617	0.599	0.621	0.613	*0.01*
Dy	4.05	4.00	3.91	3.94	3.92	*0.05*
Ho	0.862	0.838	0.820	0.820	0.815	*0.02*
Er	2.53	2.53	2.47	2.45	2.46	*0.04*
Tm	0.380	0.379	0.365	0.369	0.361	*0.01*
Yb	2.58	2.60	2.55	2.51	2.51	*0.04*
Lu	0.406	0.416	0.396	0.394	0.388	*0.01*
Hf	2.92	3.04	2.66	2.77	2.81	*0.13*
Ta	0.132	0.139	0.134	0.135	0.128	*0.00*
Pb	7.22	7.81	7.46	6.86	7.02	*0.33*
Th	4.11	4.68	3.95	4.01	4.00	*0.27*
U	1.49	1.71	1.43	1.44	1.46	*0.10*

Fe_2O_3*, total Fe as Fe_2O_3
LOI, loss on ignition

Table 2. Tridymite and glass composition.

	Tridymite				Matrix Glass	
	Average	S.D. ($n = 34$)	Min	Max	Average	S.D. ($n = 51$)
SiO2	98.05	0.59	96.77	99.26	74.85	0.63
TiO2	0.14	0.07	0.02	0.30	0.40	0.02
Al2O3	0.60	0.28	0.16	1.11	12.32	0.17
FeO	0.18	0.06	0.06	0.39	2.07	0.18
MnO	n.d.	–	–	–	0.06	0.01
MgO	n.d.	–	–	–	0.16	0.07
CaO	0.03	0.02	0.00	0.08	0.80	0.15
Na2O	0.14	0.07	0.02	0.29	2.99	0.10
K2O	0.13	0.06	0.03	0.27	5.03	0.13
P2O5	n.d.	–	–	–	0.06	0.03
Cl	n.d.	–	–	–	0.19	0.02
Total	*99.28*				*98.87*	

enhanced crystallisation prior to eruption of volcanic rocks (Higgins and Roberge 2003). The CSD of the tuffisite samples generally maintains the overall shape of the distribution, however in all samples an increase in small crystals at the expense of the population with the largest size can be observed (Figure 4).

Tridymite phase identification and composition

Within the tuffisite domains as well as the fragmental domains of the erupted ash, tridymite is an ubiquitous mineral (Figures 5 and 6), but it is completely absent in coherent magmatic domains (Figure 2E, Fig. S1).

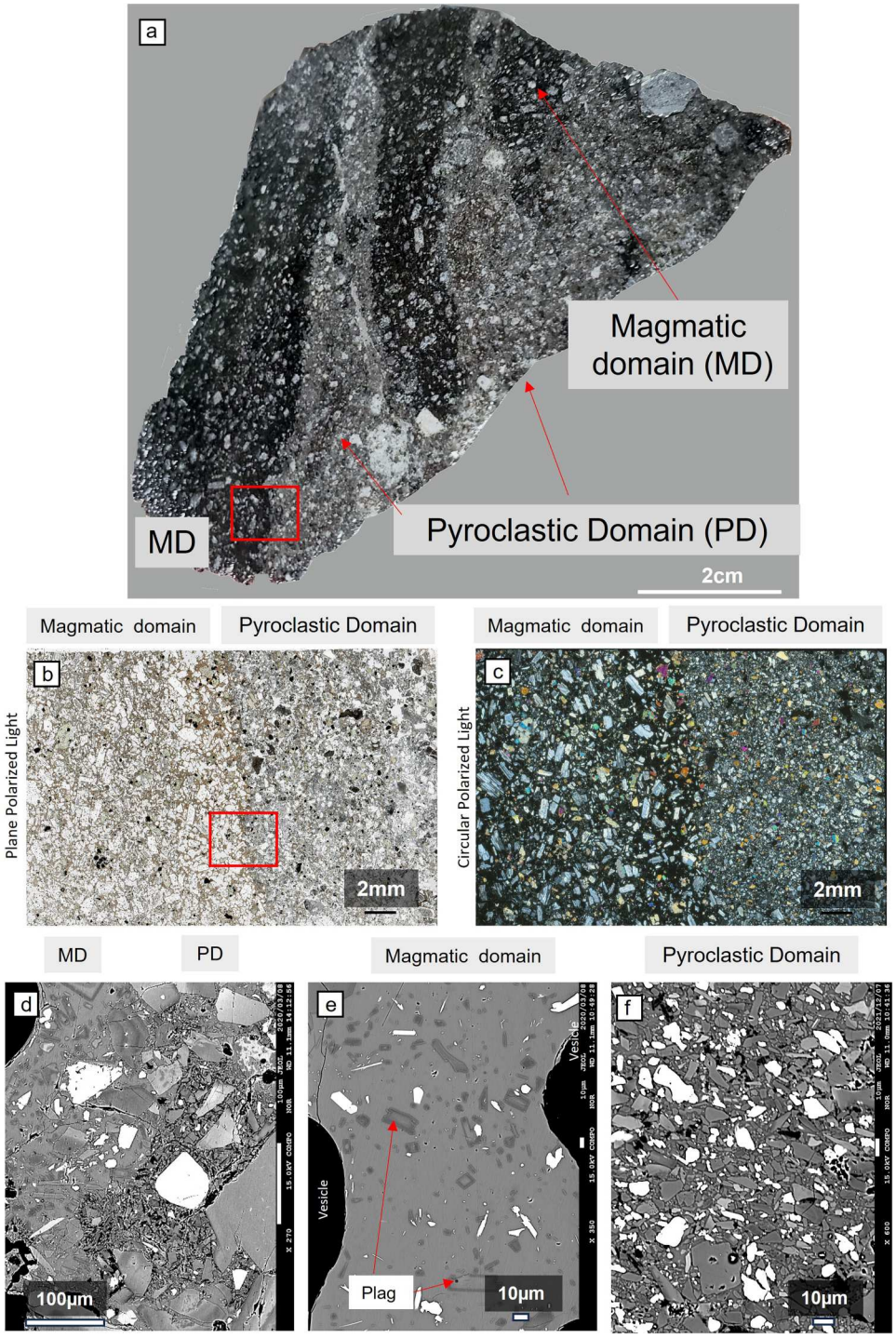

Figure 2. Tuffisite (pyroclastic domain – PD) and coherent lava (magmatic domain – MD) at different scales **A,** hand specimen with light grey tuffisite veins hosted in dark grey coherent andesite **B. C,** closeup of the contact in plane polarised light and circular polarised light. The majority of phenocrysts are plagioclase. Notice their euhedral habit in the MD and their fragmental, much smaller overall size in the PD **D,** closeup of the contact and larger individual domains **E. F,** in backscatter image.

Tridymite phase identification was done automatically by the OMNIC software database provided with the Raman Spectrometer. In addition, we downloaded standard sample spectra R160073 from the RRUFF database (Lafuente et al. 2016) for direct comparison (Figure 6B, D Supplement S5). Composition varies between 96 and 99 wt% SiO_2 and shows limited coupled Al^{3+} and $Na^{+} + K^{+}$ substitution (Figure 6G, Table 2). Such a compositional variation and degree of substitution is generally characteristic of tridymite due to the more open structure of the mineral (Deer et al. 1992) concerning pure quartz. In addition, the substitution of alkalis also has an influence on the phase stability of the different silica polymorphs (Roy and Roy 1964; Dapiaggi et al. 2015; Schipper et al. 2020; Martel et al. 2021). Individual tridymite crystals are un-zoned and show an overall homogenous composition (Figure 5D). Together with backscatter images, element maps also help to discern compositional boundaries between submicron

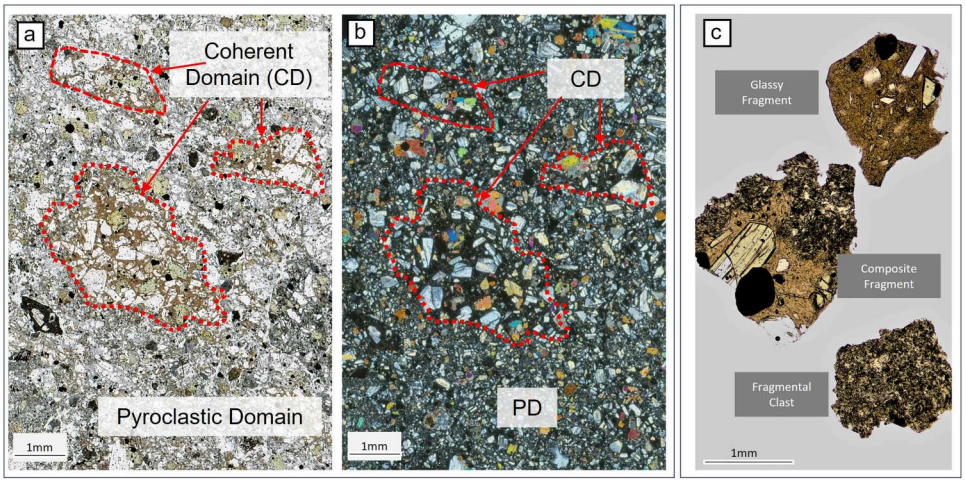

Figure 3. Closeup of Tuffisite Vein with larger glassy clasts preserved (a-plane polarised light / b – cross polarised light). Notice how plagioclase remains its euhedral habit in the glassy magmatic domains. Image c shows similar textures from the ash fraction. Notice that the composite fragment is essentially a miniature tuffisite (i.e. some coherent melt got amalgamated to a more fine-grained sintered material aggregate).

plagioclase fragments (Ca, Al-rich) and adjacent matrix glass (Al-rich – Ca-poor; see supplementary element maps – S4).

Crystals sizes range from submicron nanolites to microlites of more than 100 μm (Figure 5 and Supplement S3-S5). Tridymite crystals found in the ash samples are compositionally (Figure 6G) and texturally (Figure 5, S3) identical to the one found in the tuffisites. In the coarse and fine ash, tridymite occurs in sintered fragmental clasts and within the amalgamated sintered fragmental domains of composite ash fragments; see Figure 3 and S3. In the very fine ash fraction, tridymite can also occur as singular monomineralic fragments (S3).

Discussion

Magma fragmentation and tuffisite formation

Processes and products of magmatic fragmentation during Vulcanian explosions have been previously studied in detail (Gabellini et al. 2022) including the ability of pyrogenic minerals to record fragmentation processes (Miwa and Geshi 2012). However, in these cases the evidence for the fragmentation process is presented away from the original context (i.e. together with adjacent coherent high T magma and volatiles) under which fragmentation occurred. Tuffisites hold this additional information as they preserve context and evidence of processes that happened during and after the fragmentation event. External tuffisites have been previously reported from various geologic environments and a broad spectrum of magma compositions. In contrast, internal tuffisites are most commonly described from silica-rich, highly viscous, rhyolitic magmas (Stasiuk et al. 1996; Tuffen et al. 2003; Schipper et al. 2013; Saubin et al. 2016; Schipper et al. 2021). This observation is related to the fact that highly evolved magmas exhibit strong non-Newtonian behaviour at high strain rates and are prone to brittle failure, i.e. magmatic fragmentation under natural eruptive conditions (Webb and Dingwell 1990). Whole-rock compositions of the erupted magmas at Ebeko Volcano show andesitic or basaltic andesite compositions (Belousov et al. 2021), both magma types are usually characterised by much lower viscosities. However, the highly porphyritic nature of this magma plays a critical role in the tuffisite formation at this volcano as the large fraction of crystals is increasing magma viscosity significantly. In addition, the groundmass glass (representing the actual liquid viscosity) has a highly evolved composition. Belousov et al. (2021) calculated effective viscosities (liquid + crystal cargo) for Ebeko magmas as high as 10^8 Pa·s, well within the range of rhyolitic magmas (Lesher and Spera 2015). Unlike rhyolitic magmas, which are often crystal poor, the high crystallinity in the studied samples (47–56 vol% crystals) allows to display and quantify magma fragmentation. High strain rates during magma ascent and individual Vulcanian explosions will act upon the magma, leading to brittle failure, which in turn will also affect the crystal cargo of the magma, which is mechanically coupled to the fracturing liquid at the point of brittle failure. Thus, the crystals themselves act as a quantifiable proxy for magma fragmentation (i.e. the process would be more difficult to demonstrate in reamalgamated sintered aphyric rocks). The fragmentation effect is already apparent by visual observation (Figure 2B, C, Figure 3, S2-2 and S2-3) and further documented by the CSD variation (Figure 4) which shows the rotation of the CSD curve towards an increased proportion of fine crystals at the expense of large crystals (Higgins 2006; van der Zwan et al. 2013).

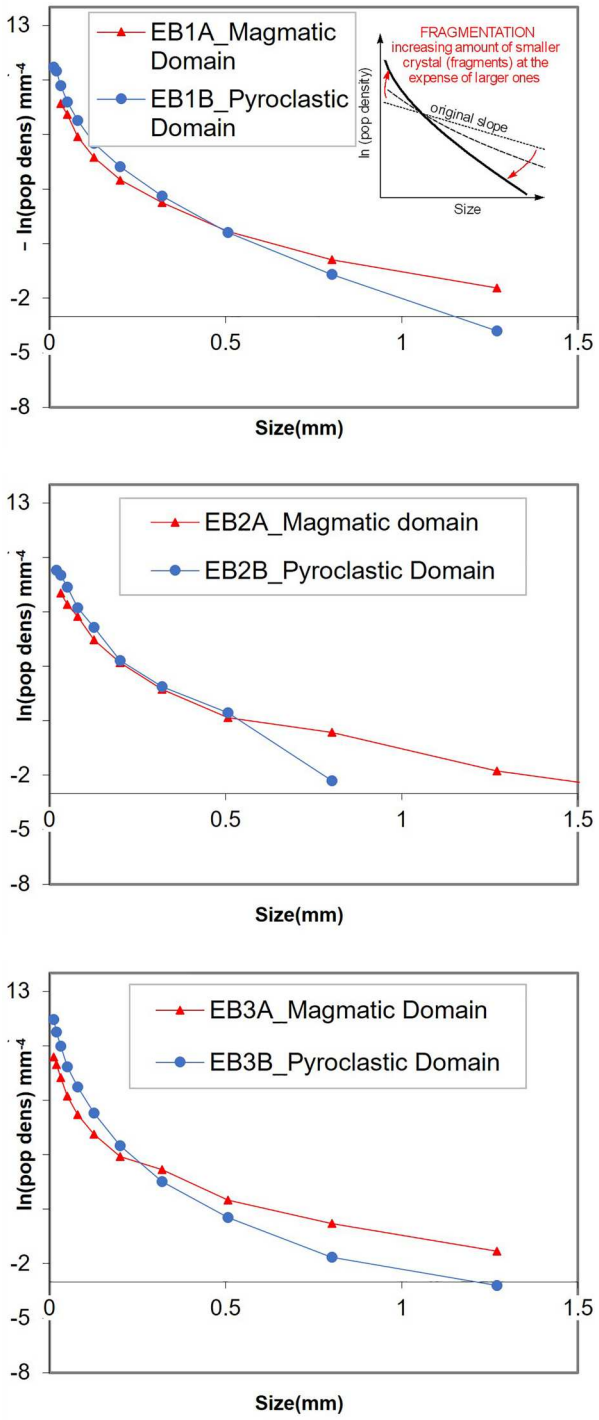

Figure 4. Crystal size distribution (CSD) for coherent lava domains and adjacent tuffisite daomains. While the overall shape of the CSD remains similar all tuffisite show and increasing number density of small crystals at the expense of the number density of the larger populations, a feature generally assigned to fragmentation processes [see inset after van der Zwan et al. (2013)].

Formation of the tuffisite (as well as the fine-grained amalgamated fragmental ash particles) must have occurred prior to final fragmentation and ejection within large bombs (for the tuffisites) or injection into the atmosphere (for the ash). This requires (at least one) additional fragmentation events prior to the final eruption (i.e. the original fragmentation that formed the pyroclasts of the tuffisite) to take place within the volcanic system. Such deep-seated 'cryptic' fragmentation has recently been proposed for silicic eruptions albeit on a much larger scale (Wadsworth et al. 2022).

We partially adopt this model of intermittent fragmentation within the deeper conduit and transient storage of tephra as it provides a feasible explanation for both tuffisite formation as well as the necessary conditions for tridymite formation (see discussion below). Like in the model by Wadsworth et al. (2022) we infer that disruption of the sealing lava cap leads to decompression and a fragmentation front that travels into the magma storage. The forthcoming explosion will eject and evacuate the uppermost storage region, but fragmentation will extend further down the conduit, where fragmental material remains after the ejection. This fragmental material will subsequently be juxtaposted with replenishment magma beneath a newly forming seal sintering the stored lower conduit pyroclastic material at approximately magmatic temperatures. Unlike the Wadsworth model tuffisite formation at Ebeko Volcano occurs on a much smaller scale and fragmentation will therefore not be all-encompassing (i.e. conduit sized) but instead produce small tuffisite bands and seams within coherent effusive domains. Also unlike the model by Wadsworth et al. (2022), the coherent domains at Ebeko Volcano are genuine magmatic domains and not previously fragmented and re-sintered material.

Silica polymorph crystallisation and stability

While quartz is generally a common phase in late stage crystallisation of silica-rich melts (Gualda and Ghiorso 2013) the formation of the high temperature polymorphs tridymite and cristobalite and their paragenesis has been debated (Roy and Roy 1964). While the respective stability limits of pure stable silica phases are well known (Heaney 1994), Deer et al. (1992) expressed doubt that tridymite can directly precipitate from magma (i.e. with a coexisting igneous liquid line of descent). This assumption was recently reinforced with an extensive experimental approach on several natural samples, none of which crystallised tridymite (Martel et al. 2021). Martel et al. (2021) review existing data on pressure and temperature-dependent pure silica phase stability but also notice that these results are generally not applicable to natural systems as the incorporation of impurities (particularly alumina and alkali metals) has a profound influence on stable and metastable phase stability within this system (Roy and Roy 1964; Deer et al. 1992; Dapiaggi et al. 2015; Schipper et al. 2020).

This is in agreement with the compositional variation of our tridymite samples, which can contain up to 1.1 wt% alumina and up to 0.3 wt% sodium and potassium (Table 2, Figure 6). These values are comparable to natural samples reported from

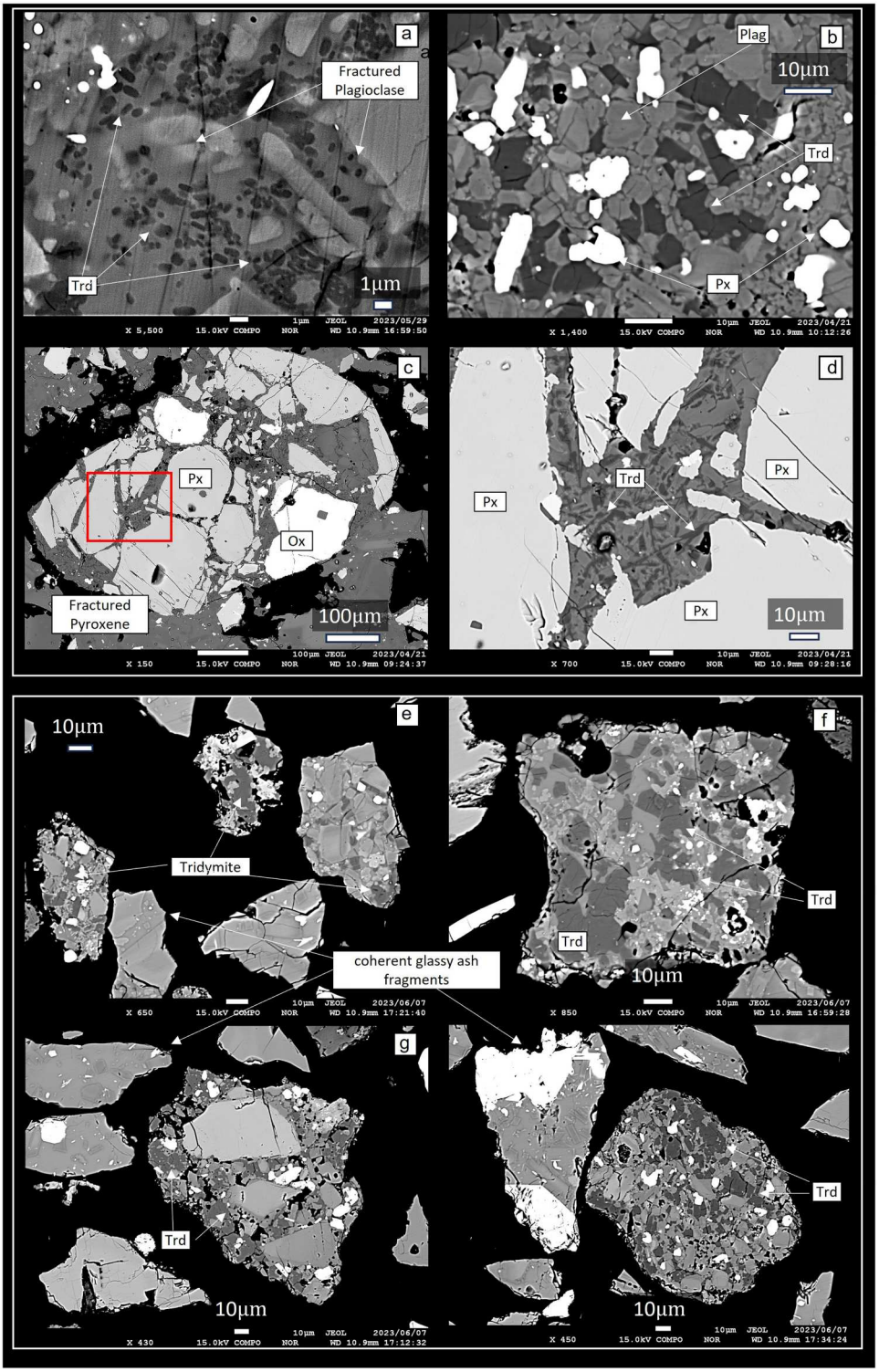

Figure 5. Tridymite in high resolution backscatter images from tuffisites (**A–D**) and erupted volcanic ash (**E–H**).

Bezymianny Volcano (Martel et al. 2021) although are slightly more potassium rich. Groundmass glass composition in our samples is rhyolitic (Table 1) and overall comparable to the natural samples reported by Martel et al. (2021) although again more potassium rich. Experiments performed near the tridymite stability field (but below 1000°C) by Martel et al. (2021) did not produce tridymite. However, they identified several experimental samples, which formed very close to the tridymite stability field. It seems conceivable that the basaltic andesites of Ebeko Volcano, with comparable high temperatures of about 1000 degree (Belousov et al. 2021) present conditions close to those required to directly crystallise tridymite from the magmatic liquid. In addition, previous studies also emphasised the importance of sodium and potassium in stabilising tridymite and cristobalite (Dapiaggi et al. 2015) with Na having a more stabilising effect on cristobalite and potassium preferentially stabilising tridymite (Martel et al. 2021).

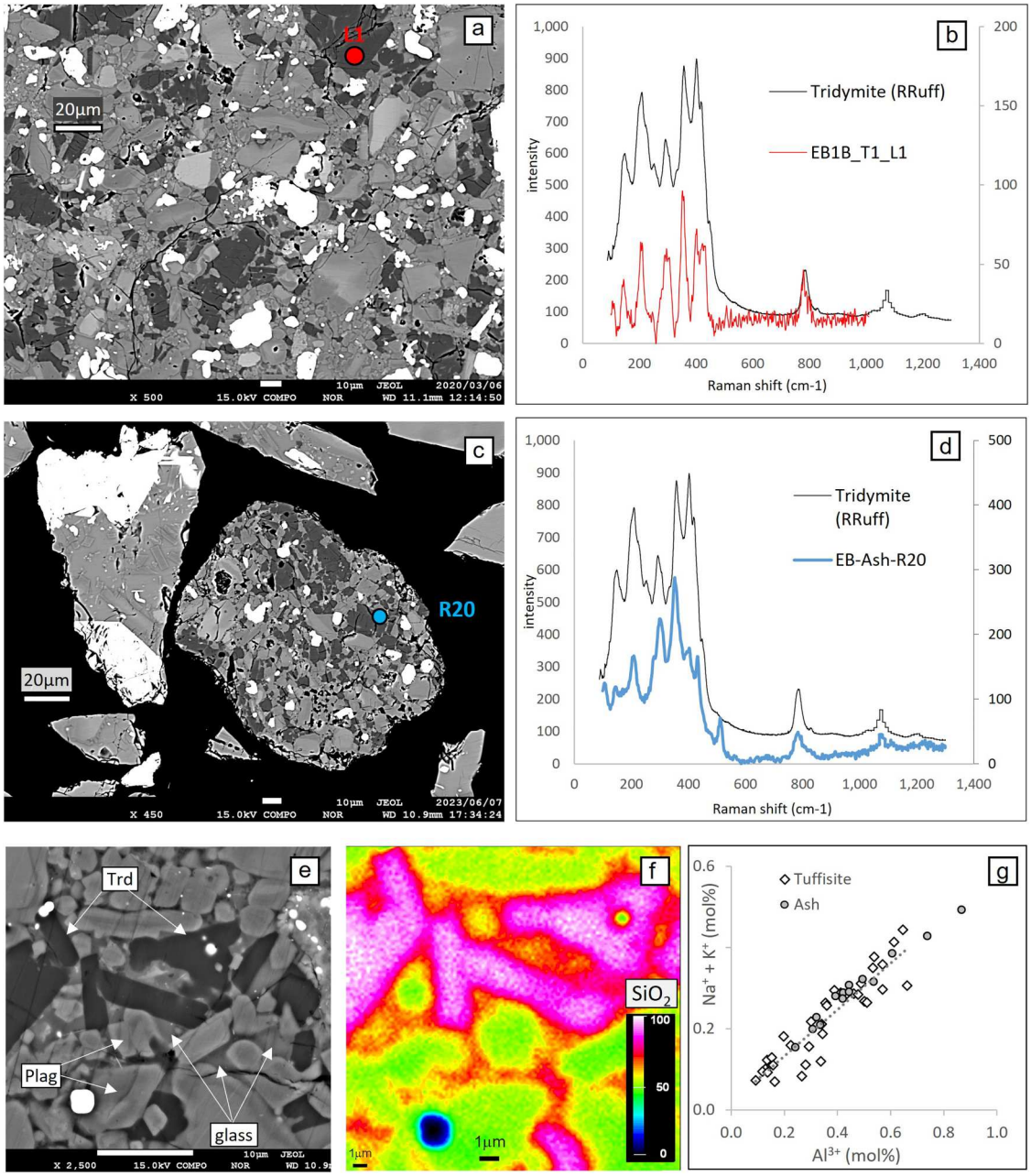

Figure 6. A. B, Tridymite phase identification and comparison with reference standard materials (RRuff database) **C. D,** Backscatter and Si-element map **E,** Coupled Al^{3+} and alkali substitution in tridymite.

However, with the exception of the tuffisites and the erupted ash, no tridymite (nor cristobalite) was found in either the lava samples or any of the magmatic domains (Figure 2E, S1). We therefore conclude that tridymite did not form as a common phase of magmatic differentiation in our samples. This also sets our samples apart from those reported by Davydova et al. (2022) where tridymite can be clearly seen within a magmatic vesicular texture.

Cristobalite as well as tridymite have been found in volcanic ash samples (Baxter et al. 1999; Horwell et al. 2013; Damby et al. 2016) and also been shown to form as products from vapour phase deposition within evolved volcanic rocks (Schipper et al. 2020; Koulakov et al. 2021). Tridymite crystallisation was also shown to occur under similar conditions when associated with cooling of silica rich ignimbrites (Heled et al. 2022). In addition, formation of silica polymorphs has been associated with the growth of silica-rich active lava domes (Hoblitt and Harmon 1993; De Hoog et al. 2005; Horwell et al. 2013; Boudon et al. 2015).

The fact that tridymite at Ebeko occurs exclusively in tuffisites and an ash samples strongly suggests involvement of a vapour phase and a causal relationship of its formation with the Vulcanian eruption process.

Tridymite crystallisation during Vulcanian explosions

While there is a substantial body of research on cristobalite vapour phase crystallisation (Schipper et al. 2020), formation of tridymite is less well studied,

however De Hoog et al. (2005) present a general model for silica precipitation and infer that the actual precipitating phase may be mainly controlled by temperature and pressure. In general, acidic volcanic gases (Cl, F) will exsolve from the magma at shallow crustal levels and partition into aqueous fluids to form acidic gas species (Aiuppa et al. 2009) with hydrofluoric acid probably of particular importance (De Hoog et al. 2005). Acidic gases will dissolve silicate which can enter the vapour phase as halogen complexes (e.g. $SiCl_4$ and SiF_4) where HF is thought to be more reactive than HCl and directly breaks Si-O bonds within the silicate frameworks allowing uptake and mobilisation of Si (Horwell et al. 2013; Schipper et al. 2017). Precipitation of SiO_2 commences when the vapour phase has become saturated in silica and an appropriate substrate is available onto which precipitation can take place. This also requires overcoming barriers to deposition that are created by lattice mismatch / lattice strain between substrate and precipitate. A large number of studies shows the formation of silica polymorphs in close association with permeable vesicle textures within otherwise coherent glassy magmatic rocks where a vapour phase percolates through permeable dome and lava structures to form silica polymorphs (Hoblitt and Harmon 1993; De Hoog et al. 2005; Horwell et al. 2013; Boudon et al. 2015; Schipper et al. 2017; Schipper et al. 2020; Davydova et al. 2022).

Such a mechanism seems to be hindered at the Vulcanian system of Ebeko Volcano for all larger coherent lava rocks (magmatic domains) domains due to their low permeability. They consequently lack any presence of silica polymorphs. Instead, in the following section we will suggest a mechanism during which fragmentation of the magma, gas exsolution and the subsequent fluid flow through stored permeable fragmental material in the upper conduit leads to the formation of tridymite.

De Hoog et al. (2005) use a (simplified) equilibrium reaction to consider the formation and stability of a SiF_4 halogen complex and the precipitation of a silica polymorph:

$$SiO_2(s) + 4HF(g) \longleftrightarrow SiF_4(g) + 2H_2O(g)$$

They show that the equilibrium of the reaction is strongly shifted to the left side of the equation during decompression where SiO_2 and HF become the stable phases. While temperature decrease generally shifts the equilibrium to the right side of the equation, the overall effect of temperature was shown to be negligible if considering natural volcanic systems. They thus conclude that decompression can play an important role in the precipitation of silica within active volcanic systems.

Vulcanian systems are characterised by the repeated sealing / pressurisation of the magmatic conduit and subsequent explosion / fragmentation and eruption (e.g. see Figure 4 in Walter et al. 2020). During each individual explosion decompression of the system will lead to gas exsolution, magma fragmentation and partial evacuation of the upper conduit forming a Vulcanian eruption plume. However, additional new pyroclastic material will form in the deeper conduit (cryptic fragmentation) and presumably also line the conduit walls and partially remain in the upper conduit. Parts of this fragmental material will be entrained within subsequent recharge magma and exposed to magmatic temperatures (sintering). During closure of the system a pressurised pocket of magma + ash-laden gas will accumulate within the conduit (Muramatsu et al. 2023). The equilibrium process proposed by De Hoog et al. (2005) suggests that during this stage, silica uptake as a silica halogen complex will be the dominant mechanism. The most likely source for such a process is finely fragmented glassy material (Figure 7A). Localised corrosion seen in some of the ash and tuffisite samples (S3-3) suggests that silica scouring is happening in the upper conduit. Following explosion and decompression equilibrium will shift to the left side of the equation leading to the precipitation of tridymite among previously fragmented material (Figure 7B). As long as the low-pressure state remains and silica-bearing fluids percolate the upper conduit tridymite crystallisation and growth can continue (7C). Following the subsequent closure of the system a new cycle will begin. Lack of permanent geophysical monitoring of the volcano makes it difficult to estimate a precise depth range for the proposed processes. However, we infer them to operate within approximately 0–2 km depth, based on comparable eruptions on similar volcanic systems (Takagi et al. 2005) A recent study by Sakurai et al. (Sakurai et al. 2024) has shown that (at least for cristobalite) halogens are not essential for the precipitation of silica. If this is also the case for tridymite and alternative possibility could be that gas ascending from larger depth is already silica rich. Since the size of tridymite crystals observed in our samples ranges from sub-micron to several tens of micrometers the conditions for crystallisation may vary possibly depending on not only the subsurface storage duration, suitable sintering conditions but also actual state of the volcanic system.

The timescale between fragmentation, particle capture and fracture healing / sintering is unknown but at least in some cases assumed to be short. Evidence for this assumption is given by the proximity of fragmented clasts of various size. Figure 5A shows fractured plagioclase crystals, which remain '*in situ*' after breakage. Figures 5C and D show a large pyroxene phenocryst within a tuffisite domain, that has been fragmented and subsequently invaded by a surrounding fluid phase and tridymite has started to form.

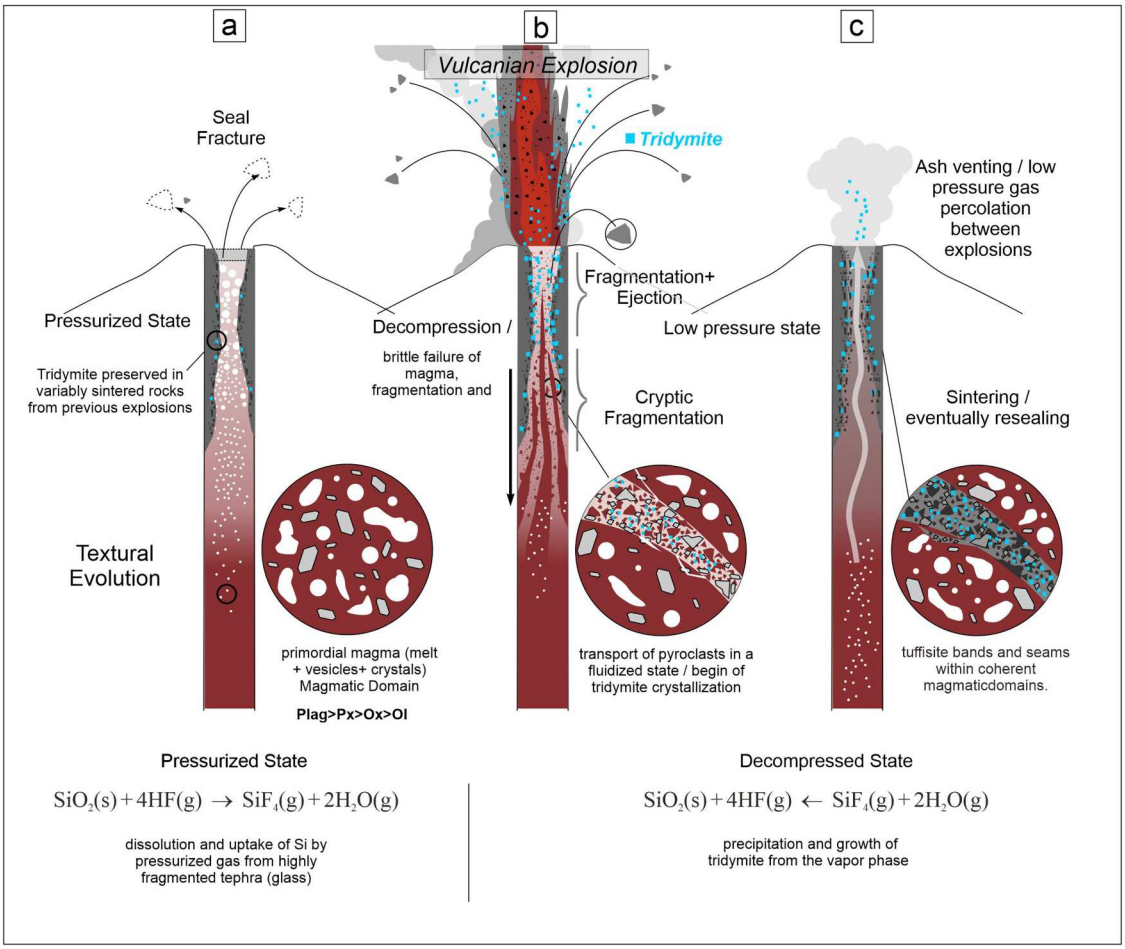

Figure 7. A, the original magma phase assemblage does not contain any silica polymorph. It is however repeatedly pressurised in the upper magmatic together with fragmental material from previous eruptions. Muramatsu et al. (2023) show how highly pressurised 'gas pockets' can form under such conditions. Such conditions promote silica dissolution and stability of silica halogen complex **B,** Decompression and Fragmentation allow for precipitation of tridymite which may continue to grow as long as gas and ash venting resumes under low pressure conditions **C,** before the system becomes sealed again and a new explosive cycle commences.

However, the crystal largely remains in its original position with a jigsaw fit texture and the interstitially precipitated tridymite is small.

The formation and stability of silica polymorphs at active volcanic systems has been a topic of intensive research for many decades (see a detailed review in Martel et al. 2021). It is not immediately obvious why at Ebeko Volcano, tridymite crystallised instead of cristobalite. One noticeable difference are the overall relatively high magmatic temperatures. Belousov et al. (2021) presented a detailed study on mineral chemistry and phase equilibria from the recent Ebeko eruption and discuss applicability of several geothermobarometers. They show that the most appropriate estimate for an eruption temperature can be made based on the equilibrium between groundmass orthopyroxene and matrix glass. The respective calculations yield an eruptive temperature of ca. 1000 degree C (Belousov et al. 2021). Another apparent difference is the slightly higher potassium content of the magmatic liquid.

Previous studies have shown that highly evolved silica-rich lava domes provide a suitable environment for the formation of silica polymorphs, where a vapour phase percolates through permeable, vesicular, glassy dome rock material. Magma ascent within the Vulcanian system of Ebeko Volcano does not provide such conditions. However, sufficient permeability is created following magma fragmentation where significant silica-rich gas flux can percolate through highly permeable ash and tuffisite and precipitate the silica polymorph tridymite. Additional studies at similar Vulcanian systems may provide more insights and answers to this question.

Conclusion

Explosive volcanic activity leads to the fragmentation of magma, which produces pyroclasts of variable size. Due to the inherent danger of explosive eruptions insights into the underlying process is either gained from analogue experiments, modelling or from

observation of the erupted products. In the case of the latter – if present – tuffisites can provide a more immediate perspective on magmatic fragmentation as they preserve the products of fragmentation (i.e. the tephra) within additional context of its formation. Because the samples observed in this study are very crystal rich, the phenocrysts themselves were used as a quantifiable proxy to document magma fragmentation. The phenocryst assemblage between coherent (unfragmented) lava samples and pyroclastic material is identical, with the exception of tridymite, which is only present in the erupted ash and the tuffisite veins. Tridymite does not crystallise from the evolved magmatic liquid but forms as a consequence of explosive eruptive activity and volatile exsolution and fluid flow following decompression and magma fragmentation. It will therefore be present in the erupted tephra, but lacking in all coherent magmatic rocks. The tuffisite samples are an exception which preserves the circumstances of the appearance of this new phase.

Our results suggest that a portion of pyroclastic particles during Vulcanian outbursts is not ejected in the atmosphere immediately after the magma fragmentation. Instead, fragmental material can spend time trapped inside pyroclast-filled veins of the volcanic plug (these veins, if later recaptured by coherent lava, form tuffisite domains). During temporary storage between succeeding explosions (tentatively from a few hours to days), before final ejection into the atmosphere, newly as well as previously fragmented pyroclastic material will be stored under conditions that allow for tridymite formation due to decompression and gas flux through the upper crustal tephra storage.

Unlike the highly permeable effusive rocks of evolved silica-rich lava domes, at Ebeko Volcano, permeability for gas flux and silica polymorph formation is caused by magmatic fragmentation. Compared with typical (dome-forming) Andesitic – Dacitic Pelean eruptions, the overall higher temperatures of the magmatic system at Ebeko, are favouring the formation of tridymite over cristobalite during VPC.

Acknowledgments

This paper presents results of a joint research program carried out at the Institute for Planetary Materials, Okayama University, supported by 'Joint Usage / Research Center' program by MEXT, Japan. We thank Ivan Koulakov for discussion about the magmatic system of Ebeko Volcano. Anjikar Ajinkya Deepak and Hiroyuki Nomori are thanked for help processing the Raman data.

Data availability statement

The supplementary material was uploaded to the 'figshare' webpage under the following DOI: -Additional images: S1-5: 10.6084/m9.figshare.27645789. -Additional data S6: 10.6084/m9.figshare.27645819.

Disclosure statement

No potential conflict of interest was reported by the author(s).

ORCID

Andreas Auer http://orcid.org/0000-0002-4387-8353

References

Aiuppa A, Baker DR, Webster JD. 2009. Halogens in volcanic systems. Chem Geol. 263(1–4):1–18. doi:10.1016/j.chemgeo.2008.10.005.

Alidibirov M, Dingwell DB. 1996. Magma fragmentation by rapid decompression. Nature. 380(6570):146–148. doi:10.1038/380146a0.

Baxter PJ, Bonadonna C, Dupree R, Hards VL, Kohn SC, Murphy MD, Nichols A, Nicholson RA, Norton G, Searl A. 1999. Cristobalite in volcanic ash of the soufriere hills volcano, Montserrat, British west indies. Science. 283(5405):1142–1145. doi:10.1126/science.283.5405.1142.

Baxter PJ, Searl AS, Cowie HA, Jarvis D, Horwell CJ. 2014. Evaluating the respiratory health risks of volcanic ash at the eruption of the Soufriere Hills Volcano, Montserrat, 1995 to 2010. Geol Soc Lond Mem. 39(1):407–425. doi:10.1144/M39.22.

Belousov A, Belousova M, Auer A, Walter TR, Kotenko T. 2021. Mechanism of the historical and the ongoing Vulcanian eruptions of Ebeko volcano, Northern Kuriles. Bull Volcanol. 83(1):1–24. doi:10.1007/s00445-020-01426-z.

Boudon G, Balcone-Boissard H, Villemant B, Morgan DJ. 2015. What factors control superficial lava dome explosivity? Sci Rep. 5(1):14551. doi:10.1038/srep14551.

Cashman KV, Scheu B. 2015. Magmatic fragmentation. In: Sigurdsson H, editor. The Encyclopedia of Volcanoes. 2nd ed. London: Academic Press; p. 459–471. doi:10.1016/B978-0-12-385938-9.00025-0.

Clarke AB, Ongaro TE, Belousov A. 2015. Chapter 28 - Vulcanian eruptions. In: Sigurdsson H, editor. The Encyclopedia of Volcanoes. 2nd ed. London: Academic Press; p. 505–518. doi:10.1016/B978-0-12-385938-9.00028-6.

Cloos H. 1942. Bau und Tätigkeit von Tuffschloten: Untersuchungen an dem Schwäbischen Vulkan. Geol Rundsch. 32(6–8):709–800. doi:10.1007/BF01801913.

Damby DE, Murphy FA, Horwell CJ, Raftis J, Donaldson K. 2016. The in vitro respiratory toxicity of cristobalite-bearing volcanic ash. Environ Res. 145:74–84. doi:10.1016/j.envres.2015.11.020.

Dapiaggi M, Pagliari L, Pavese A, Sciascia L, Merli M, Francescon F. 2015. The formation of silica high temperature polymorphs from quartz: influence of grain size and mineralising agents. J Eur Ceram Soc. 35(16):4547–4555. doi:10.1016/j.jeurceramsoc.2015.08.015.

Davydova VO, Shcherbakov VD, Plechov PY, Koulakov IY. 2022. Petrological evidence of rapid evolution of the magma plumbing system of Bezymianny volcano in Kamchatka before the December 20th, 2017 eruption. J Volcanol Geotherm Res. 421:107422. doi:10.1016/j.jvolgeores.2021.107422.

Deer WA, Howie RA, Zussman J. 1992. An introduction to the rock-forming minerals. [place unknown]: Longman Scientific & Technical Hong Kong.

Degterev AV, Chibisova MV. 2022. Volcanic activity of the Kuril Islands in 2020–2021. Geosystems Transit Zones. 6(3):195–205. doi:10.30730/gtrz.2022.6.3.195-205.

De Hoog JCM, Van Bergen MJ, Jacobs MHG. 2005. Vapour-phase crystallisation of silica from SiF4-bearing volcanic gases [Internet]. [accessed 2023 Jun 9]. https://www.earth-prints.org/handle/2122/938.

Gabellini P, Cioni R, Geshi N, Pistolesi M, Miwa T, Lacanna G, Ripepe M. 2022. Eruptive dynamics and fragmentation mechanisms during cyclic Vulcanian activity at Sakurajima volcano (Japan): insights from ash texture analysis. J Volcanol Geotherm Res. 428:107582. doi:10.1016/j.jvolgeores.2022.107582.

Gualda GA, Ghiorso MS. 2013. Low-pressure origin of high-silica rhyolites and granites. J Geol. 121(5):537–545. doi:10.1086/671395.

Heaney PJ. 1994. Chapter 1. Structure and chemistry of the low-pressure silica polymorphs. In: Heaney PJ, Prewitt CT, Gibbs GV, editors. Silica: Physical behavior, geochemistry, and materials applications. Berlin, Boston: De Gruyter; p. 1–40. doi:10.1515/9781501509698-006.

Heled Y, Rowe MC, Chambefort I, Wilson CJN. 2022. Significance of tridymite distribution during cooling and vapor-phase alteration of ignimbrites. Am Mineral. 107(3):460–475. doi:10.2138/am-2021-7814.

Higgins MD. 2000. Measurement of crystal size distributions. Am Mineral. 85(9):1105–1116. doi:10.2138/am-2000-8-901.

Higgins MD. 2006. Quantitative textural measurements in igneous and metamorphic petrology. [place unknown]: Cambridge university press.

Higgins MD. 2010. Imaging birefringent minerals without extinction using circularly polarized light. Can Mineral. 48(1):231–235. doi:10.3749/canmin.48.1.231.

Higgins MD, Roberge J. 2003. Crystal size distribution of plagioclase and amphibole from Soufriere Hills Volcano, Montserrat: evidence for dynamic crystallization–textural coarsening cycles. J Petrol. 44(8):1401–1411. doi:10.1093/petrology/44.8.1401.

Hoblitt RP, Harmon RS. 1993. Bimodal density distribution of cryptodome dacite from the 1980 eruption of Mount St. Helens, Washington. Bull Volcanol. 55(6):421–437. doi:10.1007/BF00302002.

Horwell CJ, Michnowicz S, Le Blond J. 2008. Report on the mineralogical and geochemical characterisation of chaitén ash for the assessment of respiratory health hazard. Int Volcan Health Hazard Netw. 1–36.

Horwell CJ, Williamson BJ, Llewellin EW, Damby DE, Blond L, S J. 2013. The nature and formation of cristobalite at the Soufrière Hills volcano, Montserrat: implications for the petrology and stability of silicic lava domes. Bull Volcanol. 75(3):696. doi:10.1007/s00445-013-0696-3.

Imai N, Terashima S, Itoh S, Ando A. 1995. 1994 compilation values for GSJ reference samples, "igneous rock series". Geochem J. 29(1):91–95. doi:10.2343/geochemj.29.91.

Imai N, Terashima S, Itoh S, Ando A. 1999. 1998 compilation of analytical data for five GSJ geochemical reference samples: the "instrumental analysis series. Geostand Newsl. 23(2):223–250. doi:10.1111/j.1751-908X.1999.tb00576.x.

Kendrick JE, Lavallée Y, Varley NR, Wadsworth FB, Lamb OD, Vasseur J. 2016. Blowing off steam: tuffisite formation as a regulator for lava dome eruptions. Front Earth Sci. 4:41. doi:10.3389/feart.2016.00041.

Koulakov I, Plechov P, Mania R, Walter TR, Smirnov SZ, Abkadyrov I, Jakovlev A, Davydova V, Senyukov S, Bushenkova N. 2021. Anatomy of the Bezymianny volcano merely before an explosive eruption on 20.12. 2017. Sci Rep. 11(1):1–12. doi:10.1038/s41598-021-81498-9.

Kuno H. 1950. Petrology of Hakone Volcano and the adjacent areas, Japan. GSA Bull. 61(9):957–1020. doi:10.1130/0016-7606(1950)61[957:POHVAT]2.0.CO;2.

Lafuente B, Downs RT, Yang H, Stone N. 2016. 1. The power of databases: The RRUFF project. In: Armbruster T, Danisi RM, editors. Highlights in Mineralogical Crystallography. Berlin, München, Boston: De Gruyter (O); p. 1–30. doi:10.1515/9783110417104-003.

Lesher CE, Spera FJ. 2015. Chapter 5 - Thermodynamic and transport properties of silicate melts and magma. In: Sigurdsson H, editor. The Encyclopedia of Volcanoes. 2nd ed. London: Academic Press; p. 113–141. doi:10.1016/B978-0-12-385938-9.00005-5.

Lu Y, Makishima A, Nakamura E. 2007. Coprecipitation of Ti, Mo, Sn and Sb with fluorides and application to determination of B, Ti, Zr, Nb, Mo, Sn, Sb, Hf and Ta by ICP-MS. Chem Geol. 236(1–2):13–26. doi:10.1016/j.chemgeo.2006.08.007.

Makishima A, Nakamura E. 2006. Determination of major/minor and trace elements in silicate samples by ICP-QMS and ICP-SFMS applying isotope dilution-internal standardisation (ID-IS) and multi-stage internal standardisation. Geostand Geoanalytical Res. 30(3):245–271. doi:10.1111/j.1751-908X.2006.tb01066.x.

Martel C, Dingwell DB, Spieler O, Pichavant M, Wilke M. 2000. Fragmentation of foamed silicic melts: an experimental study. Earth Planet Sci Lett. 178(1):47–58. doi:10.1016/S0012-821X(00)00062-5.

Martel C, Dingwell DB, Spieler O, Pichavant M, Wilke M. 2001. Experimental fragmentation of crystal- and vesicle-bearing silicic melts. Bull Volcanol. 63(6):398–405. doi:10.1007/s004450100157.

Martel C, Pichavant M, Carlo D, Champallier I, Wille R, Castro G, Devineau JM, Davydova K, Kushnir VO, R A. 2021. Experimental constraints on the crystallization of silica phases in silicic magmas. Bull Volcanol. 62(1):egab004. doi:10.1093/petrology/egab004.

Miwa T, Geshi N. 2012. Decompression rate of magma at fragmentation: inference from broken crystals in pumice of vulcanian eruption. J Volcanol Geotherm Res. 227–228:76–84. doi:10.1016/j.jvolgeores.2012.03.003.

Muramatsu D, Aizawa K, Yokoo A, Tameguri T, Iguchi M. 2023. Vulcanian eruption processes inferred from volcanic glow analysis at Sakurajima volcano, Japan. Bull Volcanol. 85(7):41. doi:10.1007/s00445-023-01656-x.

Nguyen TT, Kitagawa H, Pineda-Velasco I, Nakamura E. 2020. Feedback of slab distortion on volcanic arc evolution: geochemical perspective from late cenozoic volcanism in SW Japan. J Geophys Res Solid Earth. 125(10):e2019JB019143. doi:10.1029/2019JB019143.

Noguchi S, Toramaru A, Nakada S. 2008. Groundmass crystallization in dacite dykes taken in unzen scientific drilling project (USDP-4). J Volcanol Geotherm Res. 175(1–2):71–81. doi:10.1016/j.jvolgeores.2008.03.037.

Roy DM, Roy R. 1964. Tridymite-cristobalite relations and stable solid solutions. Am Mineral J Earth Planet Mater. 49(7–8):952–962.

Sakurai R, Nakamura M, Okumura S, Mujin M, Nakatani T. 2024. Vapor-phase crystallization from a hydrous silicate melt: an experimental simulation of diktytaxitic texture. Contrib Mineral Petrol. 179(3):23. doi:10.1007/s00410-024-02105-4.

Saubin E, Tuffen H, Gurioli L, Owen J, Castro JM, Berlo K, McGowan EM, Schipper CI, Wehbe K. 2016. Conduit dynamics in transitional rhyolitic activity recorded by tuffisite vein textures from the 2008–2009 Chaitén Eruption. Front Earth Sci. 4:59. doi:10.3389/feart.2016.00059.

Schipper CI, Castro JM, Kennedy BM, Tuffen H, Whattam J, Wadsworth FB, Paisley R, Fitzgerald RH, Rhodes E, Schaefer LN. 2021. Silicic conduits as supersized tuffisites: clastogenic influences on shifting eruption styles at Cordón Caulle volcano (Chile). Bull Volcanol. 83:1–22. doi:10.1007/s00445-020-01423-2.

Schipper CI, Castro JM, Tuffen H, James MR, How P. 2013. Shallow vent architecture during hybrid explosive–effusive activity at Cordón Caulle (Chile, 2011–12): evidence from direct observations and pyroclast textures. J Volcanol Geotherm Res. 262:25–37. doi:10.1016/j.jvolgeores.2013.06.005.

Schipper CI, Mandon C, Maksimenko A, Castro JM, Conway CE, Hauer P, Kirilova M, Kilgour G. 2017. Vapor-phase cristobalite as a durable indicator of magmatic pore structure and halogen degassing: an example from White Island volcano (New Zealand). Bull Volcanol. 79(10):74. doi:10.1007/s00445-017-1157-1.

Schipper CI, Rickard WDA, Reddy SM, Saxey DW, Castro JM, Fougerouse D, Quadir Z, Conway C, Prior DJ, Lilly K. 2020. Volcanic SiO2-cristobalite: A natural product of chemical vapor deposition. Am Mineral. 105(4):510–524. doi:10.2138/am-2020-7236.

Spieler O, Kennedy B, Kueppers U, Dingwell DB, Scheu B, Taddeucci J. 2004. The fragmentation threshold of pyroclastic rocks. Earth Planet Sci Lett. 226(1):139–148. doi:10.1016/j.epsl.2004.07.016.

Stasiuk MV, Barclay J, Carroll MR, Jaupart C, Ratté JC, Sparks RSJ, Tait SR. 1996. Degassing during magma ascent in the Mule Creek vent (USA). Bull Volcanol. 58:117–130. doi:10.1007/s004450050130.

Takagi A, Fukui K, Fujiwara K, Ueda Y, Iijima S, Yamamoto T, Sakai T, Kanno T, Katayama H. 2005. Magma supply system of the 2004 eruption at Asama Volcano estimated by crustal deformation data. Kazan. 50(5):363–375.

Terashima S, Taniguchi M, Mikoshiba M, Imai N. 1998. Preparation of two new GSJ geochemical reference materials: Basalt JB-1b and coal Fly Ash JCFA-1. Geostand Newsl. 22(1):113–117. doi:10.1111/j.1751-908X.1998.tb00550.x.

Tuffen H, Dingwell DB, Pinkerton H. 2003. Repeated fracture and healing of silicic magma generate flow banding and earthquakes? Geology. 31(12):1089–1092. doi:10.1130/G19777.1.

Unwin HE, Tuffen H, Phillips E, Wadsworth FB, James MR. 2021. Pressure-driven opening and filling of a volcanic hydrofracture recorded by tuffisite at Húsafell, Iceland: A potential seismic source. Front Earth Sci. 9:347. doi:10.3389/feart.2021.668058.

Unwin HE, Tuffen H, Wadsworth FB, Phillips ER, James MR, Foster A, Kolzenburg S, Castro JM, Porritt LA. 2023. The exposed Mule Creek vent deposits record the structure of a volcanic conduit during a hybrid explosive–effusive eruption. Bull Volcanol. 85(5):1–22. doi:10.1007/s00445-023-01638-z.

Wadsworth FB, Llewellin EW, Castro JM, Tuffen H, Schipper CI, Gardner JE, Vasseur J, Foster A, Damby DE, McIntosh IM. 2022. A reappraisal of explosive–effusive silicic eruption dynamics: syn-eruptive assembly of lava from the products of cryptic fragmentation. J Volcanol Geotherm Res. 432:107672. doi:10.1016/j.jvolgeores.2022.107672.

Walter TR, Belousov A, Belousova M, Kotenko T, Auer A. 2020. The 2019 eruption dynamics and morphology at Ebeko Volcano monitored by unoccupied aircraft systems (UAS) and field stations. Remote Sens. 12 (12):1961. doi:10.3390/rs12121961.

Webb SL, Dingwell DB. 1990. Non-Newtonian rheology of igneous melts at high stresses and strain rates: experimental results for rhyolite, andesite, basalt, and nephelinite. J Geophys Res Solid Earth. 95(B10):15695–15701. doi:10.1029/JB095iB10p15695.

Westercamp D. 1975. Petrology of the volcanic rocks of Martinique, West Indies. Bull Volcanol. 39(2):175–200. doi:10.1007/BF02597827.

Yokoyama T, Makishima A, Nakamura E. 1999. Evaluation of the coprecipitation of incompatible trace elements with fluoride during silicate rock dissolution by acid digestion. Chem Geol. 157(3–4):175–187. doi:10.1016/S0009-2541(98)00206-X.

van der Zwan FM, Chadwick JP, Troll VR. 2013. Textural history of recent basaltic-andesites and plutonic inclusions from Merapi volcano. Contrib Mineral Petrol. 166:43–63. doi:10.1007/s00410-013-0864-7.